THE JOURNAL OF PHYSICAL CHEMISTRY C LETTERS

2008, *112,* 14696–14701
Published on Web 08/27/2008

Hybrid Pt/Au Nanowires: Synthesis and Electronic Structure

Xiaowei Teng,[†] Weiqiang Han,*[,†] Qi Wang,[‡] Long Li,[§] Anatoly I. Frenkel,[‡] and Judith C. Yang[§]

Center for Functional Nanomaterials, Brookhaven National Laboratory, Upton, New York 11973, Department of Physics, Yeshiva University, New York, New York 10016, and Department of Mechanical Engineering and Materials Science, University of Pittsburgh, Pittsburgh, Pennsylvania 15261

Received: June 20, 2008; Revised Manuscript Received: July 21, 2008

This letter reports the synthesis of a new type of noble metal/noble metal hybrid (Pt/Au hybrid nanowires) via galvanic replacement reaction between Pt nanowires and $AuCl_3$. The width of nanowire component is about 2.3 ± 0.2 nm wide, and the diameter of Au component is about 4.5 nm ± 0.8 nm. More interestingly, by using X-ray absorption spectroscopy technique, charge transfer upon hybrids formation was observed, that d-charge depletion occurred at the Pt site, accompanied by d-charge gain at the Au site. The reported methodology to synthesize Pt/Au hybrid nanowires and study of electronic structure of Pt/Au hybrids will be of great importance in catalysis and materials science.

Complex hybrid nanostructures, assembled directly from different nanocomponents which do not require organic molecular bridges, are of major scientific and technological interest as they afford a myriad of opportunities in magnetic, catalytic, optical, and biomedical applications.[1−5] By coupling components, each with its different functionalities, the hybrid nanostructures offer entirely novel properties that do not appear in their monocomponent counterparts. Many hybrid nanostructures, such as semiconductor/noble metal, semiconductor/semiconductor, noble metal/noble metal, noble metal/magnetic metal or metal oxide, and semiconductor/magnetic metal or metal oxide, recently were synthesized via the Polyol processes, photochemical routes, seeded growth, or site-selective lithographic approaches.[6−18] However, we have limited ability to finely control the size, morphology, phase-segregation, and position of the components in hybrid nanostructures, partially reflecting the structural complexity imposed by the random nucleation of the second component.

Template-directed synthesis is the important synthetic strategy, which is widely applied to control morphology and/or spatial orientation of inorganic crystals. In particular, when solid substrates act as template, nucleation and epitaxial growth of colloidal crystals will proceed via well-defined crystallographic orientations parallel to the substrates.[19,20] However, the capability of template-directed epitaxial growth has been limited, since the feature size of the colloids will be similar to the scale of substrates. Since Xia developed a templating approach via a galvanic replacement reaction, templating via galvanic replacement has been paid significant attention due to its affording researchers the ability to prepare nanostructures with well-controlled dimensions, chemical composition, and heterogeneous structure by carefully selecting the templating particles (host metals) and the cations (solute metals), which possess the higher reduction potential compared with that of host metals.[21−23] Nevertheless, only a few hybrid nanostructures have been synthesized by galvanic replacement, especially hybrids including metal nanorods or nanowires.[24−26]

Bimetallic PtAu nanomaterials are of significant interest as electro-catalysts, and as selective oxidation and dehydrogenation catalysts.[27−30] Efforts to prepare Pt/Au nanostructures have been reported; however, there have not been many such hybrid structures, especially ones encompassing nanowires.[24,26] Here, we present our facile synthesis of Pt/Au hybrids via the galvanic replacement reaction between Pt nanowires and $AuCl_3$. In contrast to the reaction between Pd nanowires and $AuCl_3$ that we earlier described,[26] here the nucleation and deposition of Au was localized to certain sites along the Pt nanowires such as tips, stacking faults and twinning boundaries, to form Pt wires/Au spheres rather than the expected Pt/Au alloy particles. More interestingly, we observed charge transfer between the Au components and Pt nanowires, wherein d-charge depletion occurs at the Pt site, accompanied by d-charge gain at the Au site.

Experimental Methods

Synthesis of Pt/Au hybrid. Pt nanowires were first synthesized by the following procedures:[31−34] sodium hexachloroplatinate (Na_2PtCl_6, 28 mg, Alfa Aesar, 99.95%) was mixed with *n*-dodecyl trimethylammonium bromide (DTAB, 60 mg, Alfa Aesar, 99%) in 5 mL of toluene. Surfactant octadecylamine (ODA, 0.4 g, Aldrich, 97%) was dissolved in 2 mL of toluene via bath sonication for 15 min. The dissolved sodium hexachloroplatinate in the toluene mixture then was reduced through the dropwise addition of a freshly prepared solution consisting of sodium tetrahydridoborate ($NaBH_4$, 12 mg, Alfa Aesar, 99%) dissolved in 2 mL of distilled water. The color of the mixture changed from brownish to black quickly, and then it was left to react for 1 h at room temperature. As the reaction stopped,

* To whom correspondence should be addressed. E-mail: whan@bnl.gov. Tel: 631-344-7073. Fax: 631-344-3093.
[†] Brookhaven National Laboratory.
[‡] Yeshiva University.
[§] University of Pittsburgh.

10.1021/jp8054685 CCC: $40.75

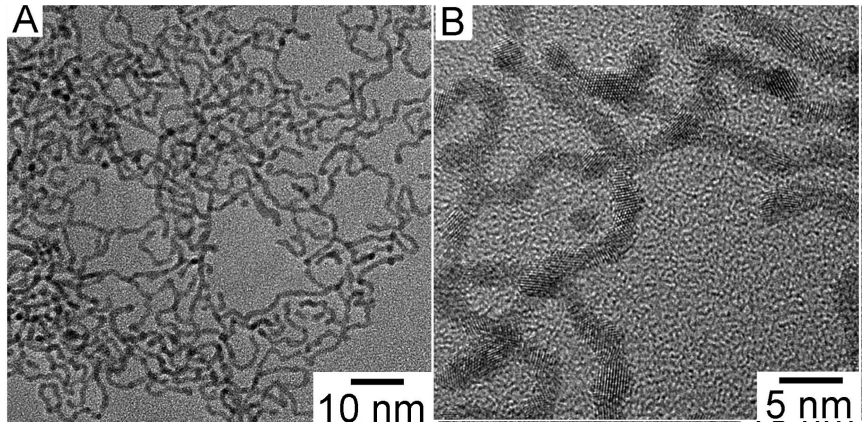

Figure 1. TEM images of Pt nanowires.

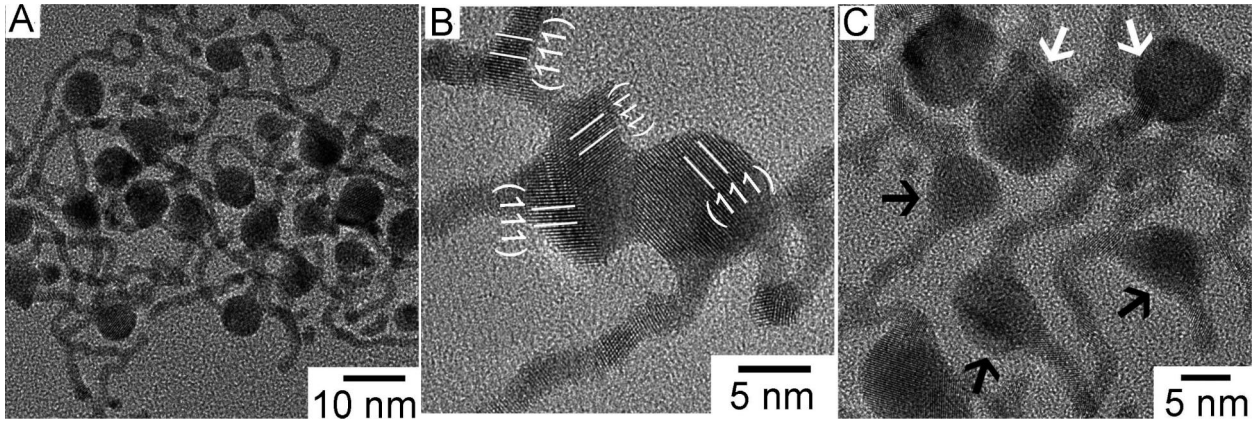

Figure 2. TEM images of (A) Pt/Au hydrids. (B,C) HRTEM images showed {111} lattice planes in both Pt and Au nanomaterials, and Au was deposited both at the tips (white arrows) and along the Pt nanowires (black arrows).

2 mL of water was added to solution. After 5 min aging, the hydrophilic phase solution containing excess amount of $NaBH_4$, if any, and phase transfer agent (DTAB) was separated from the hydrophobic phase solution. The former solution was discarded, and the latter solution that contained as-made nanomaterials was left in the flask. At the same time, $AuCl_3$ (24 mg, Alfa Aesar, 99.9%,) was dissolved in 2 mL of toluene in the presence of 30 mg of DTAB. One milliliter of $AuCl_3$ solution (0.04 mM) was then injected into freshly made Pt nanowire solution. The reaction was conducted at room temperature for one hour under argon protection. Upon completion of the reaction, the product was precipitated out by adding ethanol, followed by centrifugation, and then redispersed in chloroform.

Characterization. Specimens were prepared by dispersing the suspension of nanowires in chloroform (~1 mg/mL) and deposited on carbon-coated copper grids by drop-casting. High-resolution transmission electron microscopy (HRTEM) was performed using a field-emission JEM 3000FEG equipped with an energy dispersive spectrometry (EDS). Image acquisition and analysis was performed using Gatan Digital Micrograph. UV−vis absorption spectra were collected on a Perkin-Elmer Lambda 35 spectrometer using quartz cuvettes. High-angle annular dark field scanning transmission electron microscopy (HAADF-STEM) imaging was carried out using a JEM-2100 F (S)TEM with a field-emission gun and attached with an INCA x-Sight EDS detector. The EDS detector with a large detecting area (50 mm^2) provides high acquisition account rates. The EDS measurements were conducted under STEM mode with a beam size of 0.5 nm (nominal). X-ray absorption spectroscopy (XAS) experiments were performed at beamlines X18B and X19A at the National Synchrotron Light Source (NSLS), Brookhaven National Laboratory, Upton, New York. The storage ring energy was 2.5 GeV, and the ring current was in the range of 110−300 mA. A double-crystal Si(111) monochromator was used to scan X-ray energy from −150 to 330 eV relative to Pt L_3 edge (11564 eV) and from −150 to 1330 eV relative to Au L_3 edge (11919 eV). The high energy limit of scan ranges for the Pt L_3 and Au L_3 edges were limited by the onsets of Au L_3 and Pt L_2 absorption edges, respectively. Each sample (~10 mg) was prepared by drop-casting concentrated nanoparticles in chloroform solution onto Kapton tape evenly for adequate uniformity for XAS measurement. Standard metal (Au and Pt) foils were placed between the transmission and reference X-ray detectors and measured simultaneously with all the nanoparticle samples, for X-ray energy calibration and data alignment. Three 30 cm long ion chambers filled with suitable gas mixtures were employed to record intensity of the incident, transmitted and reference beam intensities in transmission mode for Pt edge data collection. A Lytle detector filled with Ar gas was coupled with Zn filter to measure fluorescence signal for Au edge. X-ray absorption near-edge spectroscopy (XANES) data processing was performed using the IFEFFIT package.

Results and Discussion

Figure 1 shows transmission electron microscopy (TEM) images of as-made Pt nanowires of 2.3 ± 0.2 nm wide and over 30 nm long. HRTEM observations revealed that the Pt nanowires are polycrystalline and composed of several single-crystalline elongated primary nanostructures (PNs) with high aspect ratio. PNs are interconnected either head to head or in branch-type of structures. Twinning boundaries and stacking

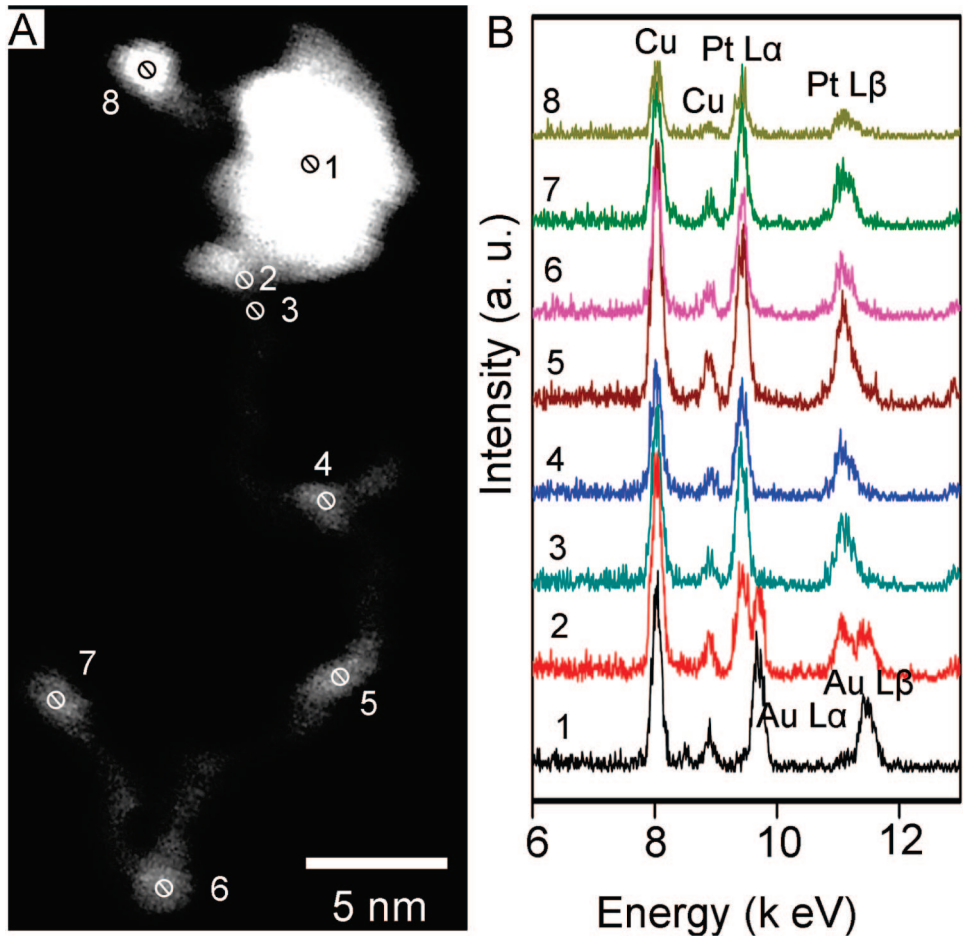

Figure 3. (A) STEM image of a Pt/Au hybrid and (B) its EDS spectra.

faults, where lattice distortion and high strain are expected, are readily seen along the nanowires.

Figure 2 shows TEM images of the Pt/Au hybrid nanowires after reacting the Pt nanowires with 2 mL of 0.04 mM $AuCl_3$ in the following galvanic replacement reaction

$$3Pt + 2Au^{3+}(aq) = 3Pt^{2+}(aq) + 2Au \quad (1)$$

The resultant hybrids were composed of elongated Pt nanostructures, and spherical Au nanoparticles of 4.5 nm ± 0.8 nm in diameter. Compared to the Pt nanowires in Figure 1, each elongated nanostructure comprised fewer single crystalline PNs, indicating an incomplete breakdown of the Pt nanowires. Even though the amount of $AuCl_3$ added sufficed to consume the entire Pt nanowires, Pt oxidation was not complete. This phenomenon was noted in other galvanic replacement reactions between Au^{3+} and Pd nanorods[24] and might be attributed to the coverage of their side surfaces by a trace amount of Au atoms or closed-packed surfactants, thereby preventing further oxidation of the Pt nanostructures during galvanic replacement. The passivation of Pt side surfaces via surfactants and/or Au atoms might also account for the fact that there were no obvious changes of the width of the Pt nanowires before and after the galvanic replacement reaction.

HRTEM images consistently showed the lattice planes for Au and Pt with lattice spacings of 2.4 and 2.3 Å, respectively, which correspond to the {111} lattice planes in both materials (Figure 2B,C). Since the mismatch of the lattice constants between Pt and Au is less than 5%, Au atoms could nucleate and grow epitaxially on the Pt nanowires along the <111> direction via attachment growth.[35,36] Moreover, as Pearson reported,[37] the Pt/Au phase diagram exhibits a miscibility gap: the solubility of Au in Pt is only about 4% at ambient temperature, rising to 6% at 973 K. Therefore, during the galvanic replacement reaction, reduced Au atoms display a strong tendency to form segregated Au particles on the Pt surfaces. This phenomenon also may be attributed to the low surface free energy of Au compared with that of Pt, thereby favoring the enrichment by Au on the Pt surfaces.

The segregation between Pt and Au is evidenced by the scanning transmission electron microscopy-energy dispersive spectroscopy (STEM-EDS) measurements shown in Figure 3. An electron spot of 0.5 nm diameter (nominal) was formed under the STEM mode and utilized to probe each site for the EDS measurements. The STEM/EDS analysis revealed compositional variation along the long axis of the hybrid nanostructures. As illustrated, the contents of Pt and Au were determined for eight sites, located at the tip and along the tail. We found that, except at the site situated in the interface between the tip and tail where both Pt and Au signals were detected (2nd site), there was distinct segregation; Au was detected only at the tip region (1st site), and Pt only was recorded in the tail region, that is, the third to the eighth site.

The chemical composition of Pt/Au hybrid also is evidenced from the ultraviolet−visible (UV−vis) absorption spectra, shown in Figure 4. As expected, no absorption peak was observed in the solution of Pt nanowires; pronounced surface-plasmon-resonance peaks characteristic of gold were obtained for the Pt/Au hybrid. Thus, this spectroscopic evidence further confirms the emergence of the Au components in the Pt/Au hybrid as the addition of $AuCl_3$ into Pt nanowires.

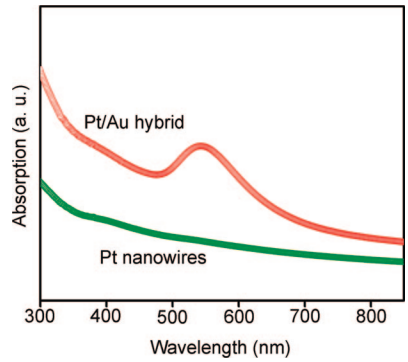

Figure 4. The UV−vis absorption spectrum of Pt nanowires and Pt/Au hybrid nanostructures.

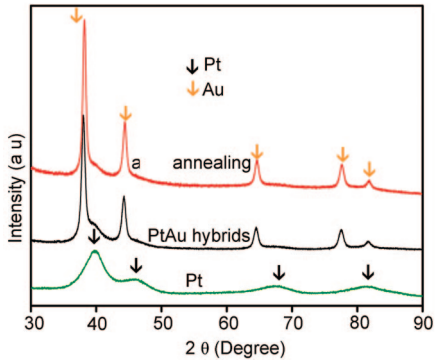

Figure 5. XRD spectrum of Pt nanowires, as-made Pt/Au hydrids, and Pt/Au hydrids after annealing at 300 °C.

The crystalline structures of Pt nanowires and Pt/Au hybrids are further studied by X-ray diffraction (XRD) measurements (Figure 5). Well-resolved, broadening peaks were observed from Pt nanowires, indexed as (111), (200), (220), and (311) diffraction peaks from the *Fm*3*m* space group. Upon the addition of $AuCl_3$, the resultant Pt/Au hybrids showed distinct two crystalline phases: broadening diffraction peaks from Pt, and narrower diffraction peaks from Au due to its larger size. The XRD data further confirmed the segregation of Au on Pt surfaces. It is interesting to note that after high-temperature (300 °C) annealing for one hour, even though the morphology of Pt/Au hydrids was totally destroyed, the complete segregation between Pt and Au still remained.

Here, we proposed a brief growth mechanism of galvanic replacement reaction between Pt and Au ions as shown in Figure 6. When $AuCl_3$ was added to the solution containing ultrathin Pt nanowires, Au^{3+} ions might preferentially attach to the certain sites along the Pt nanowires such as tips, stacking faults, and twinning boundaries, since those sites possess higher surface energy and/or relatively less passivation by surfactants due to rather sharp radius of curvature (as shown in Figure 2). Since the reduction potential of Au^{3+} to Au (E^{Φ} =1.5 V) is higher than that of Pt^{2+} to Pt (E^{Φ} = 1.2 V), Pt nanowires were oxidized and Au^{3+} ions were then reduced by the electrons generated from the replacement reaction. As the reaction continued, the Au nanoparticles grew larger, along with the consumption and breakdown of Pt nanowires. It seemed Ostwald ripening process also happened during the galvanic replacement reaction, accounting for the disappearance of smaller Au components to facilitate the growth of larger Au components. We also noticed that the ripening of Pt nanowires was not preferred, evidenced by the fact that the width of Pt nanowires did not change. The use of combined techniques such as TEM, extended X-ray absorption fine-structure (EXAFS) spectroscopy, and STEM-EDS allowed us to perform detailed analysis of the growth mechanism of Pt/Au hybrid, which will be described elsewhere.

We next turned our attention to the electronic structure of the hybrid Pt/Au nanowires. Charge redistribution occurs when heterogeneous metals react. Electrons are transferred from the metal with the more occupied valence band to the metal with the less occupied band to stabilize the bimetallic bond. X-ray absorption near-edge structure (XANES) spectroscopy, an element-specific charge state probe, is ideally suited to study the electronic structure of heterometallic materials.[38−41] We applied it to study the electronic structure of the as-made Pt/Au hybrid nanowires. Whereas metallic gold with filled d-states does not exhibit an intense peak at the L_3 absorption edge (known as the white line) compared with unfilled d9 metals (e.g., Pt), such a peak is enhanced in Au clusters when orbital s-p-d hybridization is allowed. Indeed, due to the resultant $5d^{10-x}6sp^{1+x}$ electron configuration, the density of d-holes increases leading to a potentially noticeable increase in the white line's intensity; thus, it can be used for detecting charge transfer between various heterometallic hybrid nanostructures. Furthermore, comparison of the changes in the white line's intensity at both the Pt and Au L_3 edges can serve as a sensor to detect and quantify the formation of the Pt/Au hybrid. Figure 4 plots the normalized XANES spectra from the Pt L_3 and Au L_3 edges of a Pt/Au hybrid and, for reference, those of Pt and Au foils. It shows that the intensity of the Au white line feature in the L_3 edge is noticeably lower than that of the pure Au foil. Since the white line features in the Au L_3 edge arise from $2p_{3/2}$ to $5d_{5/2}$ dipole transitions, these observations point to a decrease in the number of unoccupied states of d character at the Au site upon the dilution of the Au components in Pt nanowires. An opposite trend is apparent at the Pt L_3 edges, where the white line feature is higher than that of the pure Pt foil. These data can be further interpreted in terms of the holes population above the Fermi level, that is, the d-charge depletion at the Pt site is accompanied by the d-charge gain at the Au site. The two effects should be comparable on the basis of electronic charge neutrality.

We note that there is another possible origin of the increase in white line intensity in nanoscale materials as particle size decreases. Such effects are commonly seen in nanoscale Au, Pt clusters; they are attributed to band narrowing as the cluster size decreases.[41] However, the changes in the white line intensity in our data have a markedly different origin from the size effect. Indeed, the size effect would cause the white lines of both Au nanoparticles and Pt nanowires to increase relative to the bulk as shown in Figure 7. However, upon the formation of Pt/Au hybrids, the white line density of Au components decreased relative to the bulk and pure Au nanoparticles, indicating strongly the charge transfer between Pt and Au instead of size effect. Moreover, the charge transfer between Pt/Au in the hybrid structure appears to be very different from that in Au bimetallic alloys, such as Ag/Au, Al/Au or Ga/Au. In those alloys, the Au atoms always lose d electrons and, therefore, exhibit more intense white lines than does the in Au foil.[6,42,43] This unusual and interesting electronic behavior in Pt/Au hybrid is unexpected and deserves further exploration such as multiedges (L_1, L_2, and L_3) X-ray absorption experiments and theoretical calculations in the future.

Conclusion

We demonstrated the synthesis of a new type of Pt/Au hybrid nanowires via the galvanic replacement reaction. The nucleation

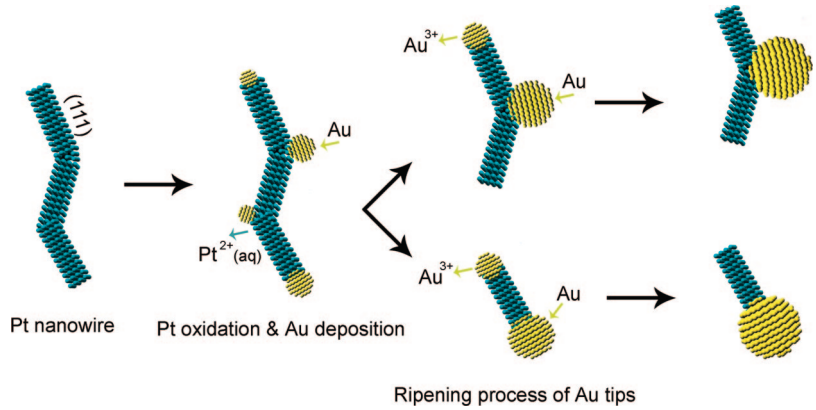

Figure 6. Schematic drawing of the galvanic replacement reaction between Pt nanowires and Au^{3+}.

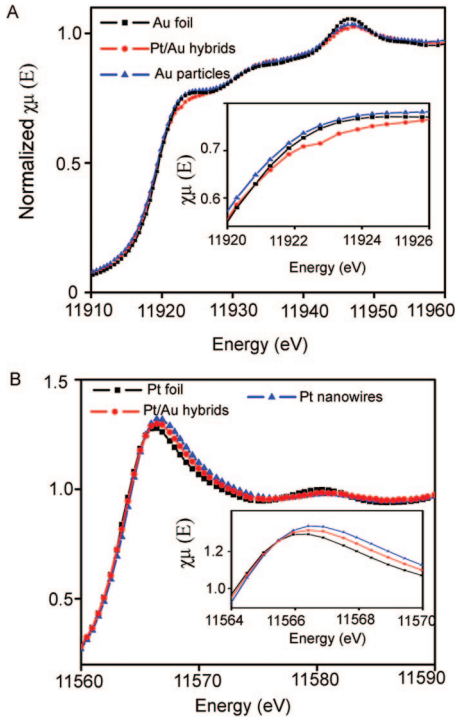

Figure 7. Normalized L_3 edge XANES spectra of (A) Au, (B) Pt in the Pt/Au hybrids, Pt nanowires, Au nanoparticles, and those of Au and Pt foils.

and growth of Au-rich nanoregions was localized to certain sites along the Pt nanowires, for example, tips, stacking faults, and twinning boundaries, to form Pt wires/Au spheres hybrids. These final hybrid structures offer a new alternative to Pt/Au alloy particles. The L_3 edge absorption of the as-made hybrids was measured via the XANES technique. We correlated the enhancement and depletion of white lines compared to those of pure elements with the charge transfer upon hybrid formation. We found that d-electron depletion occurs at Pt sites, accompanied by d-electron gain at Au sites. In this paper, we focused primarily on the details of synthesis and structural characterization of the final structure; a detailed analysis of the mechanism of hybrids formation will be reported separately. We believe the unique heterogeneous Pt/Au hybrid nanostructures and their intriguing charge-transfer properties have broad implications for designing electronic and catalytic materials and hence warrant further investigations.

Acknowledgment. This work is supported by the U.S. DOE under contract DE-AC02-98CH10886 (W.H.) and DE-FG02-03ER15476 (J.C.Y., L.L., A.I.F., Q.W.). L.L. and J.C.Y. thank Nanoscale Fabrication and Characterization Facility (NFCF) at the University of Pittsburgh. Use of the National Synchrotron Light Source, Brookhaven National Laboratory, was supported by the U.S. Department of Energy, Office of Science, Office of Basic Energy Sciences, under Contract DE-AC02-98CH10886 and beamlines X19A/X18B are partly supported by Synchrotron Catalysis Consortium under contract DE-FG02-05ER15688.

References and Notes

(1) Choi, J. S.; Jun, Y. W.; Yeon, S. I.; Kim, H. C.; Shin, J. S.; Cheon, J. *J. Am. Chem. Soc.* **2006**, *128*, 15982.
(2) Cozzoli, P. D.; Pellegrino, T.; Manna, L. *Chem. Soc. Rev.* **2006**, *35*, 1195.
(3) Wieckoweski, A.; Savinova, E. R.; Vayenas, E. G. *Catalysis and Electrocatalysis at Nanoparticle Surface*; Marcel Dekker, Inc.: New York, 2003.
(4) Zeng, H.; Li, J.; Liu, J. P.; Wang, Z. L.; Sun, S. H. *Nature* **2002**, *420*, 395.
(5) Zhang, J.; Sasaki, K.; Sutter, E.; Adzic, R. R. *Science* **2007**, *315*, 220.
(6) Buonsanti, R.; Grillo, V.; Carlino, E.; Giannini, C.; Curri, M. L.; Innocenti, C.; Sangregorio, C.; Achterhold, K.; Parak, F. G.; Agostiano, A.; Cozzoli, P. D. *J. Am. Chem. Soc.* **2006**, *128*, 16953.
(7) Ferrer, D.; Torres-Castro, A.; Gao, X.; Sepulveda-Guzman, S.; Ortiz-Mendez, U.; Jose-Yacaman, M. *Nano Lett.* **2007**, *7*, 1701.
(8) Gu, H. W.; Yang, Z. M.; Gao, J. H.; Chang, C. K.; Xu, B. *J. Am. Chem. Soc.* **2005**, *127*, 34.
(9) Gu, H. W.; Zheng, R. K.; Zhang, X. X.; Xu, B. *J. Am. Chem. Soc.* **2004**, *126*, 5664.
(10) Halpert, J. E.; Porter, V. J.; Zimmer, J. P.; Bawendi, M. G. *J. Am. Chem. Soc.* **2006**, *128*, 12590.
(11) Kudera, S.; Carbone, L.; Casula, M. F.; Cingolani, R.; Falqui, A.; Snoeck, E.; Parak, W. J.; Manna, L. *Nano Lett.* **2005**, *5*, 445.
(12) Li, Y. Q.; Zhang, G.; Nurmikko, A. V.; Sun, S. H. *Nano Lett.* **2005**, *5*, 1689.
(13) Milliron, D. J.; Hughes, S. M.; Cui, Y.; Manna, L.; Li, J. B.; Wang, L. W.; Alivisatos, A. P. *Nature* **2004**, *430*, 190.
(14) Mokari, T.; Rothenberg, E.; Popov, I.; Costi, R.; Banin, U. *Science* **2004**, *304*, 1787.
(15) Mokari, T.; Sztrum, C. G.; Salant, A.; Rabani, E.; Banin, U. *Nat. Mater.* **2005**, *4*, 855.
(16) Wetz, T.; Soulantica, K.; Talqui, A.; Respaud, M.; Snoeck, E.; Chaudret, B. *Angew. Chem., Int. Ed.* **2007**, *46*, 7079.
(17) Xiong, Y.; Washio, I.; Chen, J.; Sadilek, M.; Xia, Y. *Angew. Chem., Int. Ed.* **2007**, *46*, 4917.
(18) Zhou, S. G.; McIlwrath, K.; Jackson, G.; Eichhorn, B. *J. Am. Chem. Soc.* **2006**, *128*, 1780.
(19) vanBlaaderen, A.; Ruel, R.; Wiltzius, P. *Nature* **1997**, *385*, 321.
(20) Yin, Y.; Li, Z. Y.; Xia, Y. *Langmuir* **2003**, *19*, 622.
(21) Sun, Y. G.; Mayers, B. T.; Xia, Y. N. *Nano Lett.* **2002**, *2*, 481.
(22) Sun, Y. G.; Xia, Y. N. *Science* **2002**, *298*, 2176.
(23) Yin, Y. D.; Erdonmez, C.; Aloni, S.; Alivisatos, A. P. *J. Am. Chem. Soc.* **2006**, *128*, 12671.
(24) Camargo, P. H. C.; Xiong, Y.; Ji, L.; Zuo, J. M.; Xia, Y. *J. Am. Chem. Soc.* **2007**, *129*, 15452.
(25) Sun, Y. G.; Xia, Y. N. *J. Am. Chem. Soc.* **2004**, *126*, 3892.

(26) Teng, X.; Wang, Q.; Liu, P.; Han, W.; Frenkel, A. I.; Wen, W.; N., M.; Hanson, J. C.; Rodriguez, J. A *J. Am. Chem. Soc.* **2008**, *130*, 1093.
(27) Lang, H. G.; Maldonado, S.; Stevenson, K. J.; Chandler, B. D. *J. Am. Chem. Soc.* **2004**, *126*, 12949.
(28) Liang, H. P.; Guo, Y. G.; Zhang, H. M.; Hu, J. S.; Wan, L. J.; Bai, C. L. *Chem. Commun.* **2004**, 1496.
(29) Luo, J.; Njoki, P. N.; Lin, Y.; Wang, L. Y.; Zhong, C. J. *Electrochem. Commun.* **2006**, *8*, 581.
(30) Njoki, P. N.; Luo, J.; Wang, L. Y.; Maye, M. M.; Quaizar, H.; Zhong, C. J. *Langmuir* **2005**, *21*, 1623.
(31) Brust, M.; Walker, M.; Bethell, D.; Schiffrin, D. J.; Whyman, R. *J. Chem. Soc., Chem. Commun.* **1994**, 801.
(32) Song, Y.; Garcia, R. M.; Dorin, R. M.; Wang, H. R.; Qiu, Y.; Coker, E. N.; Steen, W. A.; Miller, J. E.; Shelnutt, J. A. *Nano Lett.* **2007**, *7*, 3650.
(33) Teng, X.; Han, W.; Ku, W.; Hücker, M. *Angew. Chem., Int. Ed.* **2008**, *47*, 2055.
(34) Wikander, K.; Petit, C.; Holmberg, K.; Pileni, M. P. *Langmuir* **2006**, *22*, 4863.
(35) Fan, F. R.; Liu, D. Y.; Wu, Y. F.; Duan, S.; Xie, Z. X.; Jiang, Z. Y.; Tian, Z. Q. *J. Am. Chem. Soc.* **2008**, *130*, 6949.
(36) Habas, S. E.; Lee, H.; Radmilovic, V.; Somorjai, G. A.; Yang, P. *Nat. Mater.* **2007**, *6*, 692.
(37) Pearson, W. B. *A Handbook of Lattice Spacings and Structures of Metals and Alloys*; Pergamon Press Ltd.: London, 1967; Vol. 2.
(38) Bus, E.; van Bokhoven, J. A. *J. Phys. Chem. C* **2007**, *111*, 9761.
(39) Frenkel, A. I.; Hills, C. W.; Nuzzo, R. G. *J. Phys. Chem. B* **2001**, *105*, 12689.
(40) Menard, L. D.; Gao, S. P.; Xu, H. P.; Twesten, R. D.; Harper, A. S.; Song, Y.; Wang, G. L.; Douglas, A. D.; Yang, J. C.; Frenkel, A. I.; Nuzzo, R. G.; Murray, R. W. *J. Phys. Chem. B* **2006**, *110*, 12874.
(41) Menard, L. D.; Xu, H. P.; Gao, S. P.; Twesten, R. D.; Harper, A. S.; Song, Y.; Wang, G. L.; Douglas, A. D.; Yang, J. C.; Frenkel, A. I.; Murray, R. W.; Nuzzo, R. G. *J. Phys. Chem. B* **2006**, *110*, 14564.
(42) Drube, W.; Treusch, R.; Sham, T. K.; Bzowski, A.; Soldatov, A. V. *Phys. Rev. B* **1998**, *58*, 6871.
(43) Watson, R. E.; Hudis, J.; Perlman, M. L. *Phys. Rev. B* **1971**, *4*, 4139.

JP8054685